Automatic Vessel Segmentation and Aneurysm Detection Pipeline for Numerical Fluid Analysis

Johannes Felde[1], Thomas Wagner[2], Hans Lamecker[1], Christian Doenitz[3],
Lina Gundelwein[1]

[1]1000shapes GmbH, Wiesenweg 10, 12247 Berlin, Germany
[2]Regensburg Center of Biomedical Engineering, OTH and University Regensburg,
Galgenbergstr. 30, 93053 Regensburg, Germany
[3]Universitätsklinikum Regensburg, Franz-Josef-Strauß-Allee 11, 93053 Regensburg,
Germany
johannes.felde@1000shapes.com

Abstract. Computational Fluid Dynamic calculations are a great assistance for rupture prediction of cerebral aneurysms. This procedure requires a consistent surface, as well as a separation of the blood vessel and aneurysm on this surface to calculate rupture-relevant scores. For this purpose we present an automatic pipeline, which generates a surface model of the vascular tree from angiographies determined by a marker-based watershed segmentation and label post-processing. Aneurysms on the surface model are then detected and segmented using shape-based graph cuts along with anisotropic diffusion and an iterative Support Vector Machine based classification. Aneurysms are correctly detected and segmented in 33 out of 35 test cases. Simulation relevant vessels are successfully segmented without vessel merging in 131 out of 144 test cases, achieving an average dice coefficient of 0.901.

1 Introduction

Intracranial aneurysms are a common cerebrovascular disease, in which a weakness of the vessel wall causes widening or ballooning of cerebral arteries. A small percentage of intracranial aneurysms rupture and consequently cause subarachnoid hemorrhage with high mortality and disability rates. Due to the catastrophic nature of aneurysm rupture on the one hand side, but low rupture risk and significant risk of complication during treatment on the other side, rupture risk assessment is an important step during clinical decision making. Different scores based on clinical, morphological and hemodynamic parameters like Normalized Wall Shear Stress (WSS) and Oscillatory Shear Index (OSI) [1] to evaluate the rupture risk, can be computed on a patient individual geometry of the vascular tract with the help of Computational Fluid Dynamics (CFD) simulations. Sufficient smoothness and resolution of the reconstructed geometry have to be ensured, to prevent introduction of non-physiological flow structures. The definition of the rupture risk scores require a differentiation between aneurysm

wall and parent vessel wall. Therefore, an aneurysm detection mechanism is required. These requirements, in combination with problems like resolution-related merging of blood vessels, pose a great challenge to the development of a fully automated segmentation pipeline for CFD analyses. Solutions that cover both problems are either semi-automatic [2] with a manual selection of seeds for a region growing, or they are only designed to detect the aneurysm and not to generate a CFD usable surface [3].

2   Methods

In this section, we describe our automatic seed extraction combined with a marker-based watershed segmentation and discuss our extension of the approach by Lawonn et al. [4] to segment and detect more complex aneurysms.

2.1   Dataset

The training data for aneurysm detection consist of 50 surface meshes provided by Pozo et al. [5] as well as 109 surface meshes from MICCAI 2020 Cerebral Aneurysm Detection challenge (CADA) [6]. The aneurysm detection and segmentation is evaluated on 35 labeled 3D Rotational Angiography (3DRA) images provided by Universitätsklinikum Regensburg (UKR). For the evaluation of the vessel segmentation, this test set is extended by 109 labeled 3DRA images from CADA challenge.

2.2   Marker-based watershed vessel tree segmentation

The vessel tree is segmented using a watershed segmentation initialized with markers defining the foreground (vessels) and background (exterior).

Skeletonization After normalizing the image data and applying an anisotropic diffusion filter to reduce image noise while preserving strong edges, the image is thresholded using an automatically calculated Otsu threshold. This results in a segmentation containing artifacts and fused vessels. A coarse vascular tree skeleton is extracted following [7] and used to mask the image data to the region of interest, accelerating the following computations.

Marker-based watershed segmentation The markers for the marker-based watershed segmentation are positioned on the large, relevant vessels of the coarse vessel tree. Therefor, the vascular tree is traversed starting from the internal carotid artery which is the vessel with the largest volume. At each node inflow direction vector v_{in} and the outflow direction vectors v_{out_n} of the incident edges are computed. Edges are grouped to vessel tracts by similar direction and radius, if they fulfill the properties: $1 - \frac{\mathbf{v_{in}} \cdot \mathbf{v_{out_n}}}{\|\mathbf{v_{in}}\| \|\mathbf{v_{out_n}}\|} > t_{cos}$ and $\frac{\bar{r}_{in}}{\bar{r}_{out_n}} < r_{ratio}$, where $t_{cos} = 0.6$ and $r_{ratio} = 0.7$ have been heuristically determined. On each vessel

tract, exceeding the empirically determined values for length of 15 mm and average radius of 2.5 mm, a marker is placed. Thin vessels that are not relevant for the CFD simulation are thus not marked and will not be segmented. The exterior marker for labeling the non exterior area is placed on a voxel with intensity 0. The marker-based watershed segmentation is computed on the gradient of the masked image resulting in a voxelwise classification with different labels for each grouped vessel.

Post-processing In order to differentiate between voxel contact areas representing touching vessel walls from those representing vessel bifurcations, we consider the local diffusion of the contact area voxels, defined by the linear diffusion C_l and planar diffusion C_p introduced by Westin et al. [8]. Assuming a more elliptical expansion for removable voxels, their C_l tends to be larger and C_p smaller than for the mostly circular cross sectioned vessel bifurcations. To determine C_l and C_p, the positions of the contact voxels are used to construct a covariance matrix with computation of singular values $\lambda_1 \geq \lambda_2 \geq \lambda_3$: $C_l = \frac{\lambda_1 - \lambda_2}{\lambda_1 + \lambda_2 + \lambda_3}$ and $C_p = \frac{2(\lambda_2 - \lambda_3)}{\lambda_1 + \lambda_2 + \lambda_3}$. The contact voxels are removed, if C_l exceeds and C_p goes below the predefined thresholds $t_{C_l} = 0.66$ and $t_{C_p} = 0.37$.

2.3   Aneurysm detection and segmentation

A modified version of Lawonn et al. [4] algorithm pipeline for detection of aneurysms based on the vascular surface geometry is used. We changed the order of the processing steps and introduced new features to the classifier to reduce false positives and ensure a stable classification of abnormal aneurysms.

Surface pre-processing The surface mesh is generated from the watershed segmentation using generalized marching cubes. To prevent possible numeric mis-calculations, it is ensured that only manifold surface parts are present.

Aneurysm candidate generation Initial binary labeling of the surface triangles $\{T_j\}$ is performed by solving the combinatorial optimization problem described in [4] using the Boykov et al. graph cut algorithm [9] based on the surface shape index [10] values S_i. A subsequent connected component analysis to group coherent triangle fields with the same label is performed. Grouped fields with aneurysm label and an average shape index $\bar{S}_i < t_S$ are discarded and labeled as vessel, where $t_S = 0.78$ is determined heuristically.

Growing of aneurysm candidates As aneurysms are not perfectly spherical, but contain concave regions as seen in Fig. 1, parts of it might be labeled as vessel. Hence, we perform an anisotropic diffusion on the aneurysm field borders, smoothing and expanding them towards the concave regions and merging close separated fields following [4]. Based on the resulting diffusion field, represented

by the continuous function $\mathbf{u}$, threshold T_{opt} assigning triangles to the aneurysm label is optimized by minimizing the length of the derived border curve. A second analysis of connected labels is performed in order to classify each grown or merged connected field in the next stage.
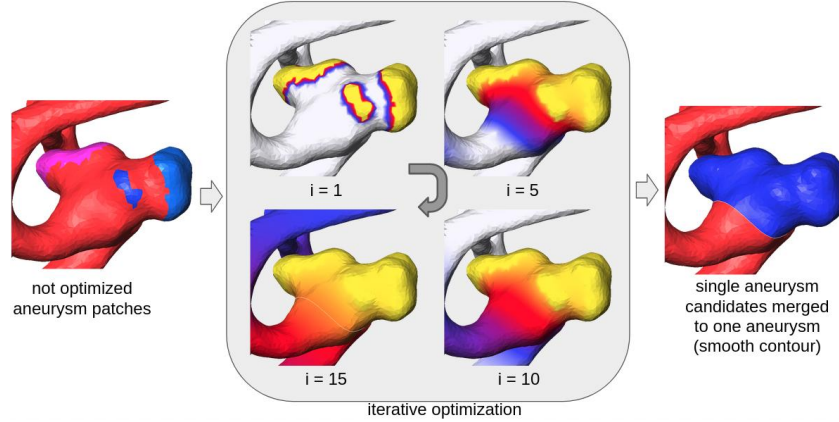

Fig. 1. Optimization of the graph cut segmented aneurysm candidate fields yields a single aneurysm with a smooth contour.

Candidate classification A Support Vector Machine (SVM) is used to reclassify the candidates in order to reduce the error rate. In total, six features are extracted from the mesh data including average shape index $\overline{S_i}$ and spherical diffusion on all field points as well as planar diffusion and linear diffusion on the field contour points, as proposed in [4]. Additionally, the variance of the shape index is used to distinguish aneurysms with both, concave and convex regions and thus similar $\overline{S_i}$ as tubular structures from vessels. Furthermore, to prevent misclassification of spherical vessel tips as aneurysms, linear diffusion of all points per field is used, exploiting the tubular characteristics of the vessels. Using mesh data of [5] and [6], 326 aneurysm candidate fields were calculated, comprising 141 aneurysm and 185 vessel fields. For each field the six features were extracted and used for a SVM training with a nonlinear RBF kernel. Optimal regularization parameter $C = 10$ and influence parameter $\gamma = 2.88$ were determined by a grid search with a 5-cross validation, achieving an accuracy of 94%. The grown candidate fields are classified with the trained SVM. Merged aneurysm fields now classified as label, probably consist of a true positive aneurysm candidate merged with a false positive and are thus separated again in a re-optimiziation process. It includes a threshold T_{limit} determination, by reducing threshold T_{opt} on $\mathbf{u}$, until the merged fields are separated. These separated fields, created by T_{limit}, are re-classified with the SVM, resulting in the final classification.

3   Results

The pipeline was qualitatively evaluated with respect to correct vessel and aneurysm segmentation on the 35 UKR cases. For quantitative evaluation of the vessel segmentation the dice value was calculated for the 35 UKR and 109 CADA cases.

3.1   Segmentation

The proposed segmentation yields dice coefficients of 0.9292 ± 0.02 for UKR and 0.8728 ± 0.043 for the more heterogeneous CADA challenge image data. 33 of 35 UKR and 98 of 109 CADA image data segmentations showed no merged vessels in simulation relevant vessels, i.e. all vessels upstream of the aneurysm as well as at least 5 times the carrier vessel diameter downstream of the aneurysm. Touching aneurysms and vessels are correctly segmented as separate structures by our algorithm, opposed to the merged structure retrieved by Otsu segementation, see Fig. 2. Generally over-segmentation rather than under-segmentation is observed.
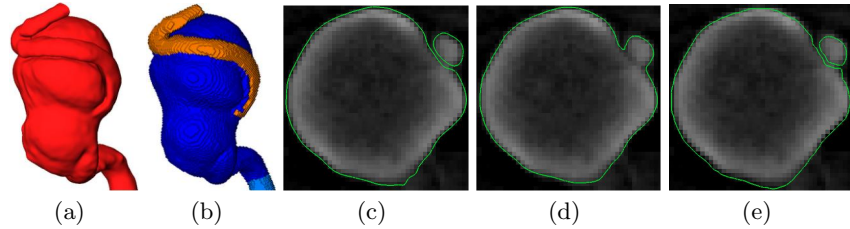

| (a) | (b) | (c) | (d) | (e) |

Fig. 2. Difficult CADA case A095 [6]: (a) Ground truth (GT) surface. (b) Proposed segmentation. (c) GT segmentation slice. (d) Otsu segmentation slice. (e) Proposed segmentation slice.

3.2   Aneurysm detection

From the 35 aneurysms, 33 were correctly detected and segmented. The aneurysms with spherical shape are easily recognized and segmented, as seen in Fig. 3(a) and 3(b), but also aneurysms with deep concave regions, are correctly segmented as a result of the improvement as seen in Fig. 3(c) and 3(d). Only two small aneurysms (see Fig. 3(e)) were not detected.

4   Discussion

We have presented a fully automated segmentation of the middle cerebral arteries and an automatic aneurysm detection resulting in surface models for CFD analysis. We segment the arterial tree with a high reliability using a marker-based watershed segmentation with subsequent separation of merged vessels. In future work we want to extend this method to fusiform aneurysms and further improve the separation of merged vessels. For the former, new features have to be
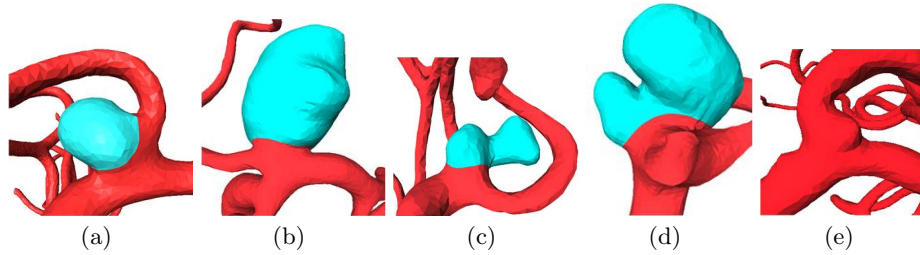
(a)   (b)   (c)   (d)   (e)

Fig. 3. Segmentation results for aneurysms with: (a) Normal sphere like structure. (b) Large sphere like structure. (c) Deep concave region. (d) Deep concave region with two sphere like blobs. (e) Missing segmentation.

added to the aneurysm detection algorithm. For the latter we plan to improve the skeletonization method which currently traces the centerline between two thin neighboring vessels, resulting in the segmentation to label them as one merged vessel tract. A recalculation of the skeleton on the watershed segmentation with a subsequent computation of a minimal spanning tree will help splitting merged vessels.

References

1. Xiang J, Natarajan SK, Tremmel M, et al. Hemodynamic–morphologic discriminants for intracranial aneurysm rupture. Stroke. 2011;42(1):144–152.
2. Seo JH, Eslami P, Caplan J, et al. A highly automated computational method for modeling of intracranial aneurysm hemodynamics. Front Physiol. 2018;9:681.
3. Rahmany I, Laajili S, Khlifa N. Automated computerized method for the detection of unruptured cerebral aneurysms in DSA images. Current Medical Imaging. 2018;14(5):771–777.
4. Lawonn K, Meuschke M, Wickenhöfer R, et al. A Geometric Optimization Approach for the Detection and Segmentation of Multiple Aneurysms. In: Computer Graphics Forum. vol. 38. Wiley Online Library; 2019. p. 413–425.
5. Pozo Soler J, Frangi AF, Consortium Tn. Database of Cerebral Artery Geometries including Aneurysms at the Middle Cerebral Artery Bifurcation. The University of Sheffield; 2017.
6. CADA challenge dataset; 2020. Available from: https://cada.grand-challenge.org/Dataset/.
7. Fouard C, Malandain G, Prohaska S, et al. Blockwise processing applied to brain microvascular network study. IEEE Trans Med Imaging. 2006;25(10):1319–1328.
8. Westin CF. Geometrical diffusion measures for MRI from tensor basis analysis. Proc ISMRM'97. 1997;.
9. Boykov Y, Veksler O, Zabih R. Fast approximate energy minimization via graph cuts. IEEE Trans Pattern Anal Mach Intell. 2001;23(11):1222–1239.
10. Koenderink JJ, Van Doorn AJ. Surface shape and curvature scales. Image Vis Comput. 1992;10(8):557–564.